ChemComm

COMMUNICATION

Heterojunction of Silver-Iron oxide on Graphene for Laser-coupled Oxygen Reduction Reaction

Wei-Quan Chen,[a] Min-Chuan Chung,[a] Joey Andrew A. Valinton,[a] David P. Penaloza Jr,[b] Shiow-Huey Chuang,[c] and Chun-Hu Chen[a]*

We reported a two-step hybridization of N-doped graphene and Ag-decorated Fe$_2$O$_3$ hematite to realize balanced oxygen adsorption/desorption equilibrium and laser-coupled ORR (LORR). Stable plateau currents with n values of 3.9 at a wide potential range (0.2-0.7 V) and 7.5% peroxide inhibition of LORR are investigated to directly associate with the Ag/Fe$_2$O$_3$ heterojunction, where interactions of semiconductor band gap excitation and plasmonic resonance-induced hot electrons are proposed to occur.

Great effort in searching for the substitute of Pt/C as inexpensive oxygen reduction reaction (ORR) electrocatalysts has been extensively focused for modern fuel cells and metal-air batteries.[1] Iron oxide catalysts featured with high abundance, excellent stability, and low environmental impacts are promising alternatives to Pt/C. But like other low-cost metal oxides, they suffer from weak energy densities and two-electron transfer ORR which generates corrosive peroxide species.[2] Apparently, combining them with mesoporous carbon materials has been reported to successfully improve the number of transferred electrons during reduction,[3] although achieving a stable limiting current remains elusive due to sluggish kinetics produced by a low electrocatalytic conversion.[4] Efficient kinetics of both oxygen adsorption/desorption needs to be achieved to address this issue.

According to the volcano curves of ORR activity, the function of oxygen binding energy over various species,[5] iron can facilitate catalytic O-O bond breaking due to strong oxygen adsorption; but this property hampers the ORR catalytic cycle because the desorption of the as-yield intermediates/products from the occupied sites becomes difficult. Silver, on the other hand, possess a relatively weak oxygen adsorption affinity,[6] which benefits intermediate/product elimination; but O$_2$ immobilization for effective catalysis becomes difficult. Our rational design aims to establish a well-balanced ORR system by establishing interfacial combination of Ag and Fe which promotes complementary, synergistic activities. Compared to platinum, the abundance and cost of silver are reasonable for commercial usage despite its low electron-transfer (n) values and high initial voltage losses.[7]

Recent studies demonstrated photo-assisted ORR are critical to realize light-driven fuel cells.[8] Chen and coworkers further revealed the mechanisms of Ag-Pt nanocages to inhibit peroxide through plasmon-induced hot electrons.[9] Strong surface plasmon can only be observed in noble metals and commonly absent in metal oxide materials. Hence, noble metals become the usual materials considered for light-assisted ORR studies.[10] Exploring usage of alternative light-excitation routes on low-cost metal oxide materials towards enhancing ORR is highly desirable but less established. In addition, white, continuous light sources were commonly used in the reported photo-assisted ORR,[9-10] however, finding specific excitation remains difficult as identification of active sites remained uncertain. We thus adopted laser as light source with a very narrow bandwidth to realize specific excitation, and a smaller required power input due to the beam-concentrated nature of laser.

In this work, we report a two-step synthesis to produce Ag/Fe$_2$O$_3$/N-doped graphene nanocomposites (Ag/FNG) with a controlled formation of Ag/Fe$_2$O$_3$ heterojunction. The significantly improved ORR activity (n=3.9) and efficient kinetics with stable limiting current can be obtained, both of which were established to originate from the heterojunction sites. For the first time, these composite catalysts demonstrated their photoactivities towards peroxide suppression through laser-coupled ORR (LORR), a light-electricity co-activation process on the electrocatalysts.

Ag/FNG was prepared by refluxing the mixture of iron (II) acetate and graphene oxide (GO) in dimethylformamide (DMF), followed by the addition of silver nitrate (10% of the moles of iron) and a subsequent hydrothermal treatment at 150°C. Subsequently, the control samples of Fe$_2$O$_3$/N-doped graphene (FNG) and Ag/N-rGO were prepared similarly without Ag and Fe

precursors, respectively. The XRD patterns of Ag/FNG correspond to hematite Fe_2O_3 and metallic silver (Fig. 1a), confirming the deposition of metallic Ag rather than Ag^+ doping in iron oxide frameworks.[11] The XRD results of the control samples FNG and Ag/N-rGO agree with their hematite and Ag components, respectively. The morphology of Ag/FNG according to the acquired TEM image resembles the deposition of the finer particles (diameter 15.3 ± 0.7 nm) onto the surface of the larger, distinct ones (diameter 79.3 ± 11.6 nm) supported by graphene sheets (Fig. 1b). These particles were confirmed to be iron and silver by EDXS data (Fig. S-1†) where the corresponding mole ratios according to ICP-MS is 0.139, a slightly higher value than that of the precursor mixture. The HR-TEM characterization of the large particles (Fig. 1b-I) shows 0.27-nm lattice fringes corresponding to d_{104} of hematite Fe_2O_3. Meanwhile, the observed 0.20-nm lattice fringes on the finer particles (Fig. 1b-II) agree with d_{200} of Ag. These results clearly demonstrate the successful formation of discrete Ag/Fe_2O_3 heterojunction in Ag/FNG, highly preferred for the effective exposure of Ag-to-Fe interfaces. The XPS studies (Fig. 1c) show binding energy of Fe $2p_{3/2}$ and $2p_{1/2}$ to be 711.5 and 724.5 eV, respectively, together with the presence of satellite peak, corresponding to Fe(III).[4c] Also, the binding energies of Ag $3d_{5/2}$ and $3d_{3/2}$ at 368.8 and 374.8 eV, respectively, further verify the presence of metallic Ag.[12] The spectra of C1s indicate a reduction of graphene oxide (rGO) in Ag/FNG, while N1s deconvolution indicates nitrogen doping in rGO with graphitic (~401.6 eV), pyrrolic (~399.5 eV), and pyridinic (398.2 eV) forms (Fig. 1d), known to greatly enhance ORR activity.[13] We selected DMF, an N-containing organic solvent, for the possible formation of iron-DMF coordination complexes capable of achieving higher degrees of N doping in GO (N-rGO), which is usually accomplished using the conventional ammonia addition approach.[13b]

The ORR performance of Ag/FNG and the control samples was evaluated through cyclic voltammetry (CV) plots under O_2- and N_2-saturated alkaline solutions (Fig. 2a). The results reveal Ag/FNG possessing the largest current and most positive onset potentials at 0.92 V (vs. RHE) as compared to Ag/N-rGO (0.87 V), FNG (0.86 V), and Fe_2O_3 (0.70 V). Fe_2O_3 has much more negative onset potentials than FNG supporting the effective ORR enhancement due to N-rGO hybridization. In Fig. 2b, the linear scan voltammogram (LSV) curves of Ag/FNG demonstrate plateau currents starting at 0.6 V. The curve shapes of Ag/FNG, as well as the control samples (Fig. S-2†), remain consistent as rotation speeds are increased (400-2025 rpm) which bring more O_2 reaching the electrode surface. Ag/FNG provides greater increase in current density as compared to others while maintaining a plateau-like diffusion limiting curve. This means the catalyst is active enough to achieve higher conversion and faster diffusion kinetics. Ag/FNG demonstrated superior ORR activity and mass transport compared to the ones without Ag/Fe_2O_3 heterojunction.

The comparison of LSV and number of electron transfer among control samples is shown in Fig. 2c and d, respectively. The two-step LSV curves of Fe_2O_3 suggest two different ORR stages in the range of 0.4-0.7 V, where two-electron transfer
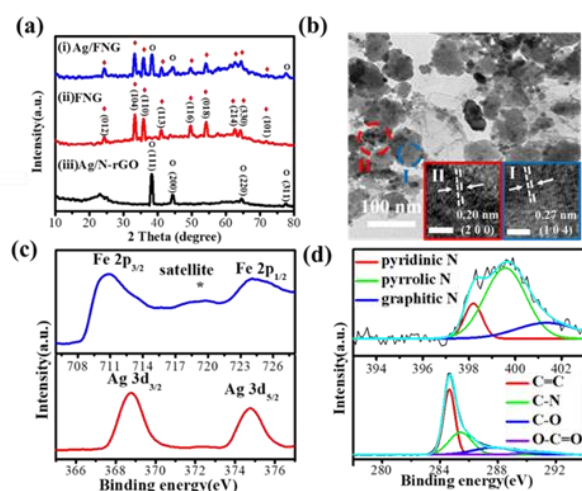

Fig. 1 - Characterization of Ag/FNG nanocomposites. (a) The comparison of XRD patterns of the nanocomposites. The red diamonds and open circles are corresponding to phases of hematite Fe2O3 and metallic Ag, respectively. (b) TEM images of Ag/FNG. The insets of high-resolution images correspond to the circle area labelled as I and II. The scale bars in the insets have a measure of 2 nm. (c) The XPS data of Ag 3d and Fe 2p; and (d) C 1s and N 1s.

pathway governs the ORR at potentials above 0.6 V (Fig. 2d). Compared to Fe_2O_3, FNG shows the similar two-step LSV but, at 0.3 V, produces higher n values (3.78) and currents. N-rGO hybridization with Fe_2O_3 enhances the current densities and decreases the onset potential barrier giving the higher n values, suggesting the formation of Fe-N-C sites[14], as well as the quasi-four-electron ORR occurring from combination of electrochemical two-electron reduction and chemical disproportionation with rapid mass transfer.[15] However, the two-step-like LSV and absence of limiting currents are still observed, similar to the reported graphene/iron oxide composites.[3-4, 16] In contrast, the single-step LSV with plateau current of Ag/FNG indicates a direct four-electron transfer like that observed in benchmark Pt/C. This similarity suggests that the plateau current can be presumably associated with the balanced adsorption/desorption equilibrium exhibited by Ag. Electrochemical Impedance Spectroscopy (Fig. S-3†) shows that
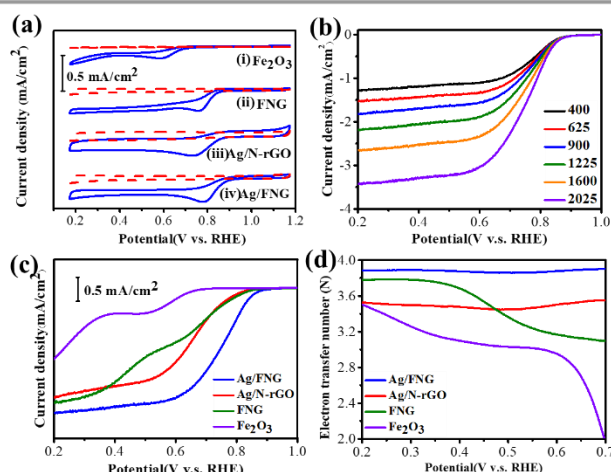

Fig. 2 - The ORR studies of Ag/FNG nanocomposites. (a) The CV comparison in 0.1 M aqueous KOH with N_2-saturated (red dashed lines) and O_2-saturated (blue solid lines) conditions. (b) LSVs of Ag/FNG in O_2-saturated 0.1 M KOH with varied rotation rates from 400 to 2025 (rpm). (c) The RDE comparison of Ag/FNG and the related samples at a rotation rate of 1600 rpm. (d) The electron transfer numbers of the samples in (c).

an increase in conductivity has been exhibited by Ag/FNG as the presence of the Ag-decorated interface with Fe_2O_3. The lowest charge transfer resistance of Ag/FNG among Ag/rGO and FNG further corresponds to the improved kinetics (Table S-1†).

Ag/FNG exhibits the greatest n values of 3.9 that remains stable over a wide potential range (0.2-0.7 V) while Ag/N-rGO draws back with relatively low n values and more negative onset potentials. Note that both hematite and FNG also show much lower n values particularly at the high potential regions (0.6-0.7 V), indicating the essential role of Ag/Fe_2O_3 heterojunction in requiring only small potential bias to realize high n values. Also, Ag/FNG only requires around 10% (i.e. 11.88%) of Ag to accomplish significant ORR enhancement which is smaller than prescribed in literature.[9] Moreover, Ag/FNG outperforms similar electrocatalysts (Table S-2) emphasizing the formation of Ag/Fe_2O_3 interfaces on graphene as an effective strategy to achieve low-cost Pt/C replacement.

To study the role of Ag/Fe_2O_3 heterojunction, an analogous control sample without Ag/Fe_2O_3 interfaces was synthesized to compare its behavior with Ag/FNG (see ESI†). The acquired TEM images show that Fe_2O_3 particles have no attachment with fine Ag dots (~5 nm, labeled by red arrows in Fig. 3a) on graphene. The XRD data confirm the presence of both metallic Ag and hematite (Fig. S-2†). The LSV results (Fig. 3b) are comparable to the two-step ORR observed in FNG, while the n values are like that of Ag/N-rGO (at 0.5-0.7 V, see Fig. 3c). Therefore, the electrocatalytic properties in this heterojunction-free catalyst sufficiently prove that the plateau current of Ag/FNG is due to the presence of Ag-Fe_2O_3 heterojunction. Also, the selective removal of Ag nanoparticles from Ag/FNG (named as Ag/FNG-Ag etched in Fig. S-3†) replaces the features of plateau currents, most positive onset potentials, and high n values as observed in Ag/FNG with these of FNG. These results clearly confirm that the Ag-Fe_2O_3 heterojunction is responsible for the greatly enhanced ORR performance.

Smaller Ag particles are generally known to exhibit the greater ORR activity.[17] To investigate whether Ag nanoparticles may solely act as the main active sites responsible for the enhanced ORR, we further narrowed down the Ag particle size in Ag/N-rGO for comparison. As shown in Fig. 3d, the Ag/N-rGO prepared under surfactant cetyltrimethylammonium bromide (CTAB) conditions, denoted as Ag/N-rGO-CTAB, yields smaller Ag particle size (5.43±2.25 nm) than Ag/N-rGO. Ag/N-rGO-CTAB reveals the more positive ORR onset potentials (0.89 V, see Fig. 3e) and the slightly smaller n values (Fig. 3f) as compared to Ag/N-rGO. These suggest that ORR activities of Ag/FNG cannot depend only on Ag particles, although Ag is critical to gain improved kinetics. Therefore Ag/Fe_2O_3 heterojunction is mainly responsible for the synergistic ORR enhancement in Ag/FNG.

We further explore the photoelectrochemical ORR of Ag/FNG under the direct laser irradiation penetrating massive water medium at room temperature (See ESI†), where drastic local heat and temperature increase at the electrodes are negligible to influence the ORR performance. The UV-vis spectra of Ag/FNG and the control samples were acquired first to identify the absorption energy among them (Fig. 4a). The bands at 269 nm (labelled by red zone) is due to $\pi \rightarrow \pi^*$ transition of

reduced graphene oxide,[18] since all the samples that contain rGO possess this band but Fe_2O_3. The shoulder band at 405 nm (labelled by blue zone) can be attributed to the band gap absorption of Fe_2O_3.[19] The surface plasmonic absorption of Ag nanoparticles is also observed in Ag/N-rGO within the blue zone.[20] Thus, the light source of 405 nm laser used in this study can both stimulate band gap excitation of Fe_2O_3 and surface plasmon of Ag. Different from the reported light sources with continuous wavelength,[9, 21] our studies of LORR behaviors can be focused on the Ag/Fe_2O_3 heterojunction only by minimizing the potential interference that comes from other parts of the composites, such as graphene material excitation. The laser-coupled LSV curves of Ag/FNG (Fig. 4b) show similar onset potentials with a higher current density than the dark condition by 12.6%. The identical onset potentials suggest no change in the active site configuration, yet the quantity of catalytically reduced oxygen is increased under the laser irradiation. Higher plateau currents in Ag/FNG reveal an increase in the oxygen molecule conversion equilibrium over time.

By comparing the difference of peroxide yields under laser-on/off conditions (Fig. 4c), the highly repeatable signals further indicate no potential decay of the photoactive sites due to laser irradiation. The laser-assisted peroxide inhibition of Ag/FNG, FNG, and Ag/N-rGO is shown to be 7.5%, 4.1%, and 2%, respectively. Moreover, the change in H_2O_2 yield of the heterojunction-free sample (Fig. S-6†) is measured to be 4.0% which is comparable to FNG. The highest inhibition capability of Ag/FNG, which is even greater than the summation of bandgap excitation (FNG) and plasmonic resonance (Ag/N-rGO), as well as the noble metal alloys,[9] reveals the strong photoelectrochemical interaction between Ag and Fe_2O_3 for peroxide depression. At the Ag/Fe_2O_3 heterojunction, the laser-excited hot electrons at Ag nanoparticles can quickly transfer to the Fe_2O_3 conduction band with the lowered Schottky barrier, as illustrated in Fig. 4d.[19, 22] Together with the photoelectrons due to laser excitation on Fe_2O_3, the localization of these charges at the interfaces makes recombination less likely to which a nearly four-electron reduction and further H_2O_2
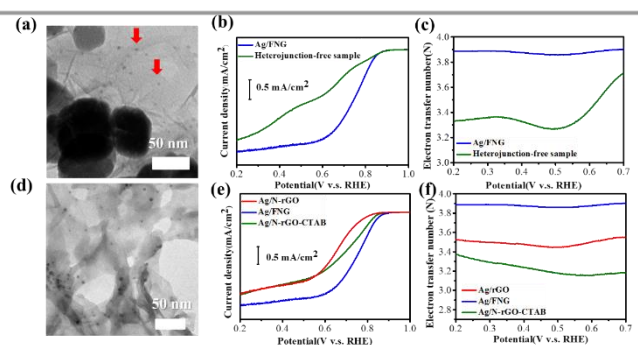

Fig. 3 - The heterojunction influence on ORR activities. (a) The TEM images of Ag/Fe_2O_3 heterojunction-free sample, and its comparison of RDE (b) and electron transfer number (c). (d) The TEM images of Ag/N-rGO-CTAB, and its comparison study of RDE (e) and electron transfer number (f).

inhibition can be attributed.[9] It is also likely that the laser-activated Ag and Fe enhances adsorption/desorption of oxygen simultaneously at the interface, which improves the mass transport and ORR kinetics for the increased plateau currents.
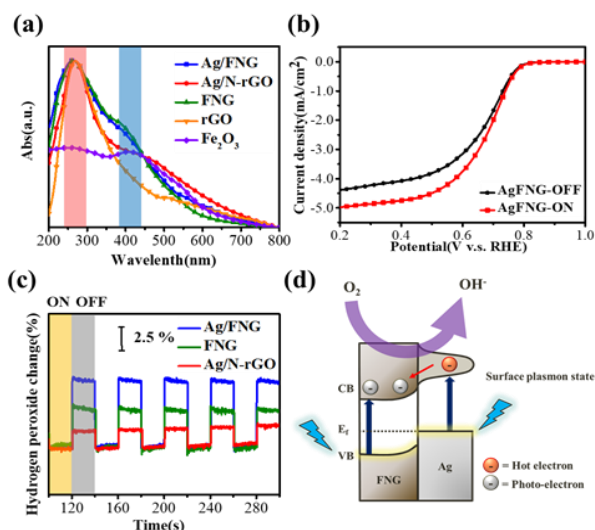
Fig. 4 - LORR studies. (a) The UV/vis spectra of all samples. (b) The RDE plots of Ag/FNG under the laser-on/off conditions at a rotation rate of 1600 rpm. (c) The changes of hydrogen peroxide yield of various samples under cyclic laser-on/off conditions. (d) The proposed LORR enhancement at the Ag/Fe$_2$O$_3$ interface.

To the best of our knowledge, Ag/FNG is the first LORR example achieving the efficient kinetics and activities realized by the specific formation of Ag/Fe$_2$O$_3$ heterojunction on graphene through the synthesis as demonstrated in this work.

In summary, we developed a two-step preparation to realize the formation of Ag/Fe$_2$O$_3$ heterojunctions on N-doped graphene, which has been experimentally confirmed as the origin of plateau currents and synergistic ORR enhancement achieving n values of 3.9 over a wide potential range with a minimized potential loss. N-doped graphene by DMF synthesis enhances the current density and lowers the onset potentials. Ag/FNG is capable of inhibiting peroxide yields under visible-light LORR, as a new example for the future design of low-cost, photo-active composite to replace noble metal electrocatalysts. The detailed mechanisms regarding photoelectrochemical ORR are currently under active investigation.

Acknowledgements

Conflicts of interest

There are no conflicts to declare.

Notes and references

1   (*a*) X. Ge, A. Sumboja, D. Wuu, T. An, B. Li, F. W. T. Goh, T. S. A. Hor, Y. Zong and Z. Liu, *ACS Catal.*, 2015, **5**, 4643-4667. (*b*) C. H. Kuo, I. M. Mosa, S. Thanneeru, V. Sharma, L. Zhang, S. Biswas, M. Aindow, S. Pamir Alpay, J. F. Rusling, S. L. Suib and J. He, *Chem. Commun.*, 2015, **51**, 5951-5954.

2   T. N. Lambert, J. A. Vigil, S. E. White, C. J. Delker, D. J. Davis, M. Kelly, M. T. Brumbach, M. A. Rodriguez and B. S. Swartzentruber, *J. Phys. Chem. C*, 2017, **121**, 2789-2797.

3   Z. S. Wu, S. Yang, Y. Sun, K. Parvez, X. Feng and K. Mullen, *J. Am. Chem. Soc.*, 2012, **134**, 9082-9085.

4   (*a*) B. Zhao, Y. Zheng, F. Ye, X. Deng, X. Xu, M. Liu and Z. Shao, *ACS Appl. Mater. Interfaces*, 2015, **7**, 14446-14455. (*b*)S. Ren, S. Ma, Y. Yang, Q. Mao and C. Hao, *Electrochim. Acta*, 2015, **178**, 179-189. (*c*) M. Sun, Y. Dong, G. Zhang, J. Qu and J. Li, *J. Mater. Chem. A*, 2014, **2**, 13635-13640.

5   J. K. Nørskov, J. Rossmeisl, A. Logadottir, L. Lindqvist, J. R. Kitchin, T. Bligaard and H. Jonsson, *J. Phys. Chem. B*, 2004, **108**, 17886-17892.

6   S.-A. Park, H. Lim and Y.-T. Kim, *ACS Catal.*, 2015, **5**, 3995-4002.

7   (*a*) F. H. B. Lima, C. D. Sanches and E. A. Ticianelli, *J. Electrochem. Soc.*, 2005, **152**, A1466. (*b*) K. Lee, M. S. Ahmed and S. Jeon, *J. Power Sources*, 2015, **288**, 261-269.

8   B. Zhang, S. Wang, W. Fan, W. Ma, Z. Liang, J. Shi, S. Liao and C. Li, *Angew. Chem., Int. Ed.*, 2016, **55**, 14748-14751.

9   S. C. Lin, C. S. Hsu, S. Y. Chiu, T. Y. Liao and H. M. Chen, *J. Am. Chem. Soc.*, 2017, **139**, 2224-2233.

10 (*a*) Y. Xiong, M. Ren, D. Li, B. Lin, L. Zou, Y. Wang, H. Zheng, Z. Zou, Y. Zhou, Y. Ding, Z. Wang, L. Dai and H. Yang, *J. Catal.*, 2017, **354**, 160-168. (*b*) L. Guo, K. Liang, K. Marcus, Z. Li, L. Zhou, P. D. Mani, H. Chen, C. Shen, Y. Dong, L. Zhai, K. R. Coffey, N. Orlovskaya, Y.-H. Sohn and Y. Yang, *ACS Appl. Mater. Interfaces*, 2016, **8**, 34970-34977. (*c*) Z. Zheng, W. Xie, M. Li, Y. H. Ng, D.-W. Wang, Y. Dai, B. Huang and R. Amal, *Nano Energy*, 2017, **41**, 233-242.

11 (*a*) C. H. Chen, E. C. Njagi, S. Y. Chen, D. T. Horvath, L. Xu, A. Morey, C. Mackin, R. Joesten and S. L. Suib, *Inorg. Chem.*, 2015, **54**, 10163-10171. (*b*) M. Özacar, A. S. Poyraz, H. C. Genuino, C.-H. Kuo, Y. Meng and S. L. Suib, *Appl. Catal., A*, 2013, **462-463**, 64-74.

12 R. Krishna, D. M. Fernandes, C. Dias, J. Ventura, E. Venkata Ramana, C. Freire and E. Titus, *Int. J. Hydrogen Energy*, 2015, **40**, 4996-5005.

13 (*a*) D. Guo, R. Shibuya, C. Akiba, S. Saji, T. Kondo and J. Nakamura, *Science*, 2016, **351**, 361-365. (*b*) W. Y. Kao, W. Q. Chen, Y. H. Chiu, Y. H. Ho and C. H. Chen, *Sci. Rep.*, 2016, **6**, 37174.

14 W. J. Jiang, L. Gu, L. Li, Y. Zhang, X. Zhang, L. J. Zhang, J. Q. Wang, J. S. Hu, Z. Wei and L. J. Wan, *J. Am. Chem. Soc.*, 2016, **138**, 3570-3578.

15 (*a*) D. A. Slanac, A. Lie, J. A. Paulson, K. J. Stevenson and K. P. Johnston, *J. Phys. Chem. C*, 2012, **116**, 11032-11039. (*b*) P. Singh and D. A. Buttry, *J. Phys. Chem. C*, 2012, **116**, 10656-10663.

16 X. Liu and W. Hu, *RSC Adv.*, 2016, **6**, 29848-29854.

17 (*a*) B. Men, Y. Sun, Y. Tang, L. Zhang, Y. Chen, P. Wan and J. Pan, *Ind. Eng. Chem. Res.*, 2015, **54**, 7415-7422. (*b*) E. J. Lim, S. M. Choi, M. H. Seo, Y. Kim, S. Lee and W. B. Kim, *Electrochem. Commun.*, 2013, **28**, 100-103.

18 Y. Zhang, H.-L. Ma, Q. Zhang, J. Peng, J. Li, M. Zhai and Z.-Z. Yu, *J. Mater. Chem.*, 2012, **22**, 13064.

19 X. Li, Z. Wang, Z. Zhang, L. Chen, J. Cheng, W. Ni, B. Wang and E. Xie, *Sci. Rep.*, 2015, **5**, 9130.

20 N. F. Adegboyega, V. K. Sharma, R. Siskova, R. Zboril, M. Sohn, B. J. Schultz and S. Banerjee, *Environ. Sci. Tech.*, 2013, **47**, 757-764.

21 Q. He, F. Zhou, S. Zhan, N. Huang and Y. Tian, *Appl. Surf. Sci.*, 2018, **430**, 325-334.

22 D. Tsukamoto, A. Shiro, Y. Shiraishi, S. Sugano, S. Ichikawa, S. Tanaka and T. Hirai, *ACS Catal.*, 2012, **2**, 599-603.

Table of Contents